ADVANCED ENERGY MATERIALS
www.advenergymat.de

Mechanism for the Fluctuation in Coulombic Efficiency of Lithium Metal Anodes After Calendar Aging

Elizabeth Zhang, Hao Lyu, Wenbo Zhang, Yuelang Chen, Philaphon Sayavong, Il Rok Choi, Yi Cui, and Zhenan Bao**

Calendar aging significantly affects lithium metal battery performance, with even short rest periods causing measurable drops in Coulombic efficiency (CE). However, most studies focus only on CE losses during rest, and the impact on subsequent cycles remains unclear. Here, calendar aging behavior is systematically examined in various carbonate and ether electrolytes, showing that aging influences not only CE after rest but also the following cycles. While all electrolytes show CE loss during rest, distinct CE patterns appear in the two post-rest cycles. To clarify the mechanism behind these fluctuations, dead lithium formation during and after aging is tracked using titration gas chromatography. This also enables quantification of CE loss associated with solid electrolyte interphase (SEI) evolution. The results indicate that the interplay between SEI evolution and dead lithium recovery governs the electrolyte-dependent CE response during post-rest cycling. Resting frequency in full cells is further varied, and it is found that increased resting frequency does not necessarily accelerate capacity loss, suggesting that rest-induced degradation is largely reversible. These findings provide insight into post-calendar aging mechanisms in lithium metal batteries and highlight the dynamic nature of rest-induced degradation.

1. Introduction

Lithium metal batteries (LMBs) show great promise for next-generation energy storage systems.[1–4] Their exceptionally high theoretical energy density makes them particularly attractive for applications such as electric vehicles and portable electronics, where maximizing energy per unit weight is critical.[5,6] Despite this potential, the practical deployment of LMBs remains hindered by several persistent challenges, particularly those related to long-term stability and efficiency.[7–9] One of the most critical challenges is understanding calendar aging—the gradual degradation that occurs when a battery is held at rest without undergoing charge or discharge cycles. A mechanistic understanding of calendar aging is fundamental for improving the lifetime and reliability of LMBs in real-world applications.

Previous studies have investigated calendar aging under both charged and discharged resting conditions,[10–16] exploring how variables such as temperature,[17] applied pressure,[18] and state of charge[19] contribute to degradation. These studies have shown that the degradation pathways are strongly influenced by the battery's rest state. For example, when the battery is rested in a charged state, lithium corrosion tends to accelerate,[12,15] leading to irreversible consumption of active lithium and a decrease in Coulombic Efficiency (CE) as the lithium reacts with the electrolyte. In contrast, when the battery is rested in a discharged state, the solid electrolyte interphase (SEI)—a passivating layer critical for lithium metal stability—can begin to dissolve.[10,11] Interestingly, this dissolution may allow previously isolated (dead) lithium to reconnect with the current collector during subsequent cycles, resulting in partial capacity recovery and a transient improvement in performance.[10]

However, most of these studies have focused primarily on the resting period itself, without thoroughly addressing what happens in the cycles that follow rest. This creates a critical gap in our understanding of the post-calendar aging effects—how rest-induced degradation continues to influence the electrochemical behavior and failure mechanisms after cycling resumes. Moreover, much of this prior work has been carried out using Li||Cu half-cell configurations, which, while useful for fundamental studies, do not fully capture the lithium-limited conditions of real-world systems. In full-cell configurations, the lithium inventory is fixed and finite, making them more sensitive to lithium loss and degradation phenomena. Although some studies have explored aging behavior in anode-free LMBs,[19,20] the

E. Zhang, W. Zhang, P. Sayavong, I. R. Choi, Y. Cui
Department of Materials Science and Engineering
Stanford University
Stanford, CA 94305, USA
E-mail: yicui@stanford.edu

E. Zhang, H. Lyu, Y. Chen, I. R. Choi, Z. Bao
Department of Chemical Engineering
Stanford University
Stanford, CA 94305, USA
E-mail: zbao@stanford.edu

Y. Chen, P. Sayavong
Department of Chemistry
Stanford University
Stanford, CA 94305, USA

Y. Cui
Stanford Institute for Materials and Energy Sciences
SLAC National Accelerator Laboratory
Menlo Park, CA 94025, USA

The ORCID identification number(s) for the author(s) of this article can be found under https://doi.org/10.1002/aenm.202504010

DOI: 10.1002/aenm.202504010

mechanisms responsible for post-aging effects remain poorly characterized, particularly in the context of full-cell operation.

In this study, we examine the long-term influence of calendar aging on LMB performance by carefully tracking the potential CE degradation pathways. We investigate three different electrolyte systems: i) LP40 (1 M $LiPF_6$ in a 1:1 volume ratio of ethylene carbonate and diethyl carbonate, a representative carbonate electrolyte), ii) 1.2 M LiFSI/F5DEE (1.2M LiFSI/2-[2-(2,2-difluoroethoxy)ethoxy]-1,1,1-trifluoroethane, a high-performing ether electrolyte),[21] iii) 2 M LiFSI/DME (2M LiFSI/dimethoxyethane, a standard ether electrolyte frequently used in LMB studies). These represent some of the most commonly tested ranges of liquid electrolytes currently being developed for lithium metal batteries.[22] We begin by evaluating cycling performance under varying resting protocols to determine how rest conditions influence long-term behavior. To better understand the underlying degradation mechanisms, we employ titration gas chromatography (TGC) to quantitatively measure the amount of dead lithium formed. This allows us to decouple the respective contributions of SEI growth and dead lithium accumulation to the overall loss in CE. Our findings show that aging effects extend beyond the rest cycle itself and can lead to fluctuation in the CE for up to two cycles after rest. The extent of these effects vary significantly based on electrolyte composition. Through our study, we propose a mechanism to explain how factors such as SEI formation, SEI dissolution, and dead lithium formation interact during and after aging to drive these CE fluctuations. Finally, we systematically investigate the impact of periodic rest in full cells using NMC811 (lithium nickel manganese cobalt oxide) as the cathode. Our findings emphasize the need for a broader understanding of calendar aging, not just during rest periods but also in their subsequent effects. This work provides crucial insights for developing strategies to reduce degradation and improve long-term LMB performance.

1.1. Electrolyte-Dependent Trends Identified with Various Calendar Aging Protocols

We first analyze cycling profiles using different resting protocols across LP40, 1.2 M LiFSI/F5DEE, and 2 M LiFSI/DME electrolyte systems. The resting frequencies tested include: i) resting every cycle, ii) resting every other cycle, iii) resting every other two cycles, and iv) resting every ten cycles. The resting time is kept at 24 h for all the conditions. The current versus time profiles of these protocols can be found in Figure S1 (Supporting Information).

For the more frequent resting protocols (every cycle and every other cycle), we found that resting not only decreased the CE in the rest cycle but also affects subsequent cycles (Figures S2–S4, Supporting Information). However, more frequent resting makes it difficult to separate individual resting effects, as cells have insufficient time to return to normal CE between rests. To better isolate resting and post-resting effects, we reduce the frequency to resting every other two cycles. To verify whether two cycles can provide enough recovery time, resting every ten cycles is also tested (Figures S2–S4, Supporting Information). This longer interval shows that resting mainly affects the two cycles immediately after rest. From the third cycle onward, we do not observe significant CE deviations from continuously cycled cells. Based on these findings, we focus our analysis on the two cycles after rest, since the protocol of resting every other two cycles proved most useful for highlighting the trends discussed in this work. **Figure 1a** shows current vs time profiles for the two protocols we used to compare the electrolytes.

This study examines three different electrolytes. Figure 1b shows cycling trends for these electrolytes in Li||Cu half cells. All cells are cycled ten times before starting periodic aging. These initial cycles help stabilize the cells and establish complete SEI formation, preventing these factors from affecting the aging study.[23] During the rest cycle itself, all three electrolytes show a noticeable drop in CE (Figure 1b). This drop follows patterns reported in previous studies,[12] where it was found that lithium metal corrodes during rest periods as it continues to react with the electrolyte.

However, the behavior during the first cycle after rest reveals intriguing differences among the three electrolytes. LP40, the carbonate-based electrolyte, shows a clear increase in CE compared to its normal cycling behavior. This unexpected improvement suggests some form of recovery mechanism. In contrast, 1.2 M LiFSI/F5DEE shows slightly lower CE compared to cells that are not rested. 2 M LiFSI/DME shows behavior somewhere between these two extremes. These varying responses suggest that each electrolyte interacts differently with the lithium metal, and this will affect the post-resting cycling performance.

The second cycle after rest reveals even more complex electrolyte-dependent patterns. In LP40 systems, we observe a decrease in CE. Noticeably, this decrease is not just a one-time effect—it becomes progressively more severe as cells go through more rest-cycle sequences. This suggests an accumulating negative impact on the cell's efficiency. The F5DEE and DME systems show the opposite behavior. Both ether-based electrolytes display increased CE during the second post-rest cycle. This improvement suggests these electrolytes might enable some beneficial processes that enhance cycling efficiency.

These observations lead to two significant conclusions about calendar aging in related lithium metal batteries. First, the effects of calendar aging extend beyond the rest cycle itself, cascading through at least two subsequent cycles. This extended influence suggests that it is necessary to think about calendar aging as a dynamic process rather than a single event.

Second, the electrolyte chemistry plays a crucial role in determining how a cell responds to rest periods. The difference observed between carbonate (LP40) and ether-based electrolytes (F5DEE and DME) suggest that strategies to minimize calendar aging effects might need to be tailored to specific electrolyte systems rather than applying a one-size-fits-all approach. To further broaden the scope of this study, we also evaluated a second ester-based electrolyte, 1 M $LiPF_6$ in EC:DMC (1:1 by volume). As shown in Figure S13 (Supporting Information), this electrolyte displayed cycling behavior very similar to LP40, with limited CE recovery and continuous dead lithium accumulation. These results further confirm that the superior recovery observed with the F5DEE/DME electrolyte is specific to ether-based systems, underscoring the strong influence of electrolyte chemistry on CE loss and recovery mechanisms.

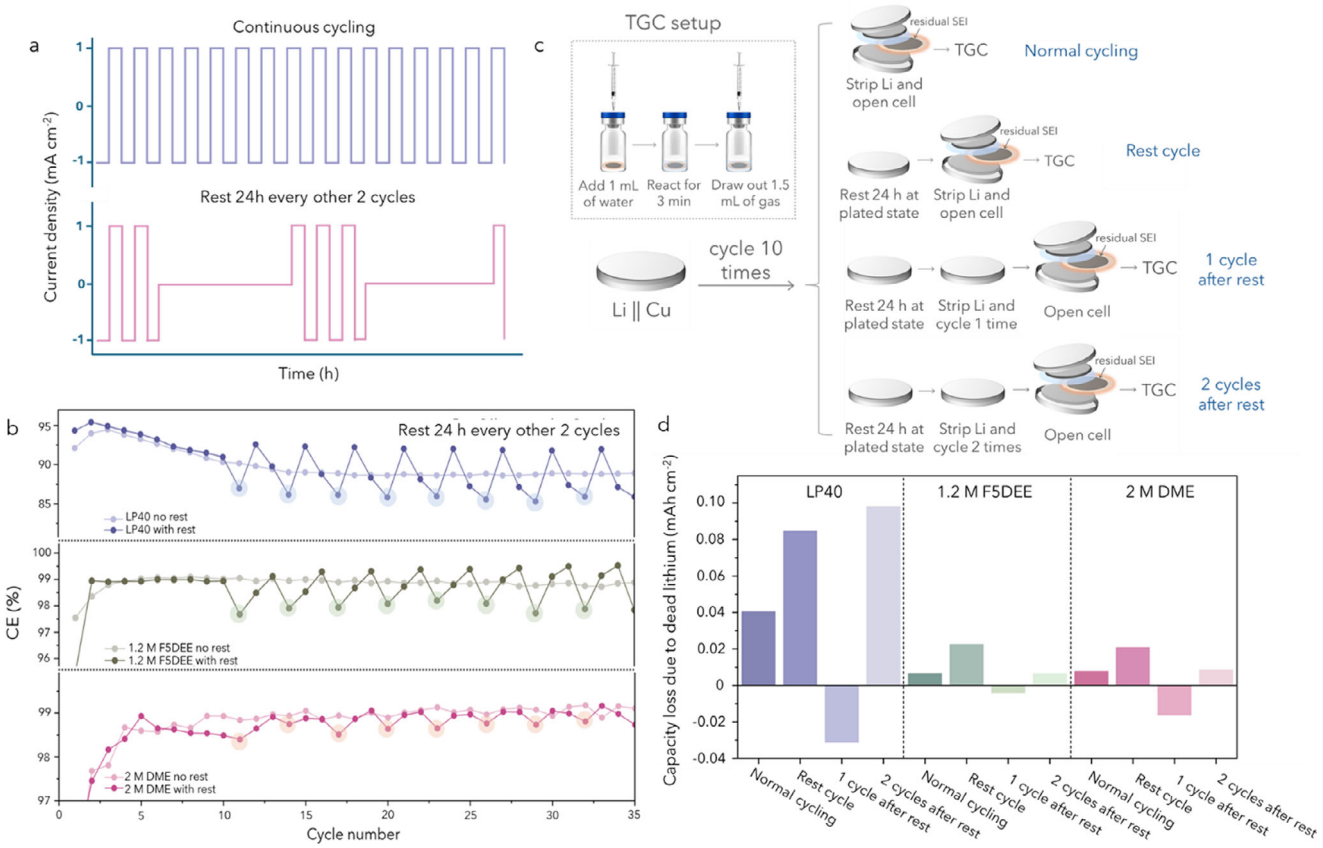

Figure 1. a) Current versus time profile of continuous cycling and rest 24 h every other two cycles. b) The Coulombic efficiency profile of Li||Cu half cells cycled at 0.5 mA cm^{-2} and 1 mAh cm^{-2}. The electrolytes tested include LP40, 1.2 M LiFSI/F5DEE, and 2 M LiFSI/DME. The cycles are cycled ten times before resting 24 h every other two cycles. The highlighted cycles are the rest cycles. c) The titration gas chromatography setup, demonstrating the four different conditions of the titrated samples. For each condition, the cells are disassembled after cycling. The copper foils with residual SEI and dead Li are titrated to obtain the reported results. d) Capacity loss due to dead lithium for the three different electrolytes. The values shown are calculated to reflect the amount formed per cycle.

1.2. Tracking Dead Li Evolution with Titration Gas Chromatography

To investigate the underlying causes of CE variations across different electrolytes, we separately investigate the two primary CE degradation mechanisms, namely dead lithium and SEI formation. Dead lithium refers to lithium that is electrically isolated during cycling, preventing it from participating in future cycles.[24] To quantify the amount of dead lithium, titration gas chromatography (TGC) is employed as the primary analytical technique.[24,25] Note that all TGC measurements are performed at fully stripped states. This ensures that the measurements capture only dead lithium, rather than any remaining active plated lithium. When dead lithium reacts with water, it quantitatively generates hydrogen gas according to the reaction: $2\ Li + 2\ H_2O \rightarrow 2\ LiOH + H_2$. By precisely measuring the amount of hydrogen generated using gas chromatography, we can back-calculate the quantity of dead lithium present in the sample. We note that the titration gas chromatography (TGC) method detects hydrogen evolution upon reaction with water, which may originate not only from metallic lithium (Li^0) but also from lithium hydride (LiH), a known component of the solid electrolyte interphase (SEI). While LiH formation has been reported in lithium metal batteries, previous studies suggest that it is unlikely to be present in very large amounts within the SEI.[26] Therefore, we expect its contribution to the total hydrogen signal to be relatively minor and not to significantly affect the observed trends in dead Li quantification. Nonetheless, we acknowledge this possible contribution as a limitation of the TGC method and an area for future investigation.

A set of resting protocols is designed based on Li||Cu half cells to systematically track dead lithium evolution through different stages of cycling and rest. Figure 1c presents a detailed scheme of the experimental process. For each electrolyte system (LP40, 1.2 M LiFSI/F5DEE, and 2 M LiFSI/DME), we prepare four distinct sets of test cells:

1) Normal cycling cells: These cells underwent tenth standard cycles (0.5 mA cm^{-2} charge and discharge, 1 mAh cm^{-2}) to establish a baseline behavior.
2) Rest cycle cells: After ten cycles, these cells were rested for 24 h in the plated state, then stripped.

3) One cycle after rest cells: After ten cycles, these cells were rested for 24 h in the plated state, then stripped, and cycled for one time.
4) Two cycles after rest cells: After ten cycles, these cells were rested for 24 h in the plated state, then stripped, and cycled for two times.

Our TGC analysis reveals several fascinating patterns in dead lithium formation. Figure 1d shows the dead lithium formation calculated for each cycle. These values are obtained by subtracting the current cycle from the subsequent cycle's dead lithium amount (i.e., the rest cycle dead lithium capacity loss value is obtained by subtracting cycle 10's cumulative dead lithium amount as determined by TGC from cycle 11). The cumulative dead lithium amount directly obtained from TGC for each test condition is also recorded in Figures S5–S7 (Supporting Information). During normal cycling conditions, we observe distinct baseline behaviors for each electrolyte. Li||Cu half cells with LP40 form ≈0.040 mAh cm^{-2} of dead lithium per cycle. This relatively high value suggests that carbonate-based electrolytes may be more prone to dead lithium formation during regular cycling.[27] 1.2 M LiFSI/F5DEE shows dead lithium formation of 0.006 mAh cm^{-2} per cycle, demonstrating improved performance compared to LP40. This lower value aligns with previous research suggesting that fluorinated ether electrolytes can help suppress dead lithium formation.[28] DME exhibited dead lithium formation of 0.008 mAh cm^{-2} per cycle, positioning it between the other two electrolytes in terms of performance. These baseline values align well with previous research indicating that most electrolytes have ≈50% of CE loss that can be attributed to dead lithium formation.[25]

After 24 h of rest, all three electrolyte systems show a substantial increase in dead lithium content—more than doubling their normal cycling values. This similar trend among the three electrolytes suggests that resting promotes dead lithium formation, regardless of electrolyte chemistry. The first cycle after rest gives more intriguing findings. At this cycle, we observe negative dead lithium capacity values. This happens when the total amount of dead lithium in the subsequent cycle is less than the current cycle. The negative dead lithium value indicates that some previously "dead" lithium becomes electrically reconnected to the conductive network. This reconnection process effectively recovers lost capacity, contributing to the CE increases we observed in our cycling data.

The second cycle after rest reveals different behaviors among the three electrolyte systems. In 1.2 M LiFSI/F5DEE and 2 M LiFSI/DME, the dead lithium amount return to their baseline level, suggesting these systems can "reset" after the perturbation of a rest period. LP40, however, shows significantly elevated dead lithium formation compared to its normal cycling behavior. This persistent increase suggests that the rest period triggers longer-lasting changes in this carbonate-based electrolyte.

To fully understand these complex behaviors, we recognize that dead lithium formation represents only part of the story. The SEI layer plays an equally crucial role in battery performance. In the following section, we will examine how the SEI evolves after resting periods to build a comprehensive model of how these two major CE loss mechanisms – dead lithium formation and SEI evolution – interact to determine overall battery performance.

1.3. Mechanism for CE Fluctuations After Calendar Aging

While the dead lithium titration experiments provide valuable insights into one aspect of calendar aging, a comprehensive understanding requires examining both dead lithium evolution and SEI behavior simultaneously. **Figure 2a–c** presents a detailed breakdown of total capacity loss, specifically separating the contributions from SEI formation and dead lithium across all three electrolyte systems during normal cycling and post-rest cycles. Note that we can obtain the SEI capacity loss by subtracting the dead lithium capacity loss (determined by TGC) from the total capacity loss. This systematic approach allows us to track how these two critical degradation mechanisms evolve throughout the aging process.

During normal cycling, all three electrolytes show a consistent pattern: ≈50% of capacity loss came from dead lithium formation. However, this changes dramatically after introducing rest periods. During the rest cycle, we observe substantial increases in dead lithium formation across all electrolytes. SEI capacity loss also shows observable increase, which can be attributed to lithium metal corrosion, where fresh lithium surfaces react with the electrolyte to form new SEI compounds.

In the first cycle after rest, all three electrolytes show recovery of previously formed dead lithium. This recovery process appears to be coupled with SEI dissolution. During rest, SEI dissolution creates opportunities for dead lithium to reconnect with the bulk lithium deposit. However, this beneficial reconnection has a trade-off: the dissolved SEI requires replacement. This necessity for SEI repair explains the increased SEI capacity loss observed during this cycle. The process resembles a "renovation" of the electrode surface, where old structures are removed and new ones form. We further note that the dissolved SEI is likely dominated by easily soluble organic species, while the repaired SEI consists of both organic and inorganic components, consistent with prior reports of SEI composition and solubility.[11]

The second cycle after rest reveals two distinct trends. First, 1.2 M LiFSI/F5DEE and 2 M LiFSI/DME both return to normal cycling levels of dead lithium formation, while LP40 shows increased dead lithium formation. Second, all three electrolytes show reduced SEI capacity loss. To explain the first observation, we recognize that dead lithium recovery must occur during normal cycling, though not as noticeably as in the rested case. Electrolytes forming large amounts of dead lithium, like LP40, likely recover small amounts each cycle. Aging causes additional dead lithium recovery in the subsequent cycle, leaving less recoverable dead lithium in the SEI matrix. This explains why LP40 shows an increased dead lithium amount after rest. This effect is less significant for 1.2 M LiFSI/F5DEE and 2 M LiFSI/DME, which form less dead lithium. For the second observation, we note that the previous cycle's SEI repair benefits the current cycle. Due to the extensive SEI formation after rest, less SEI capacity loss occurs in the second cycle after rest. This applies across all three electrolytes since they all experience significant SEI formation after rest.

Based on our observations of dead lithium and SEI capacity loss during and after aging, we present a comprehensive mechanistic model in Figure 2d. This model tracks CE recovery and loss mechanisms across four critical cycles: normal cycling, rest cycle, first cycle after rest, and second cycle after rest.

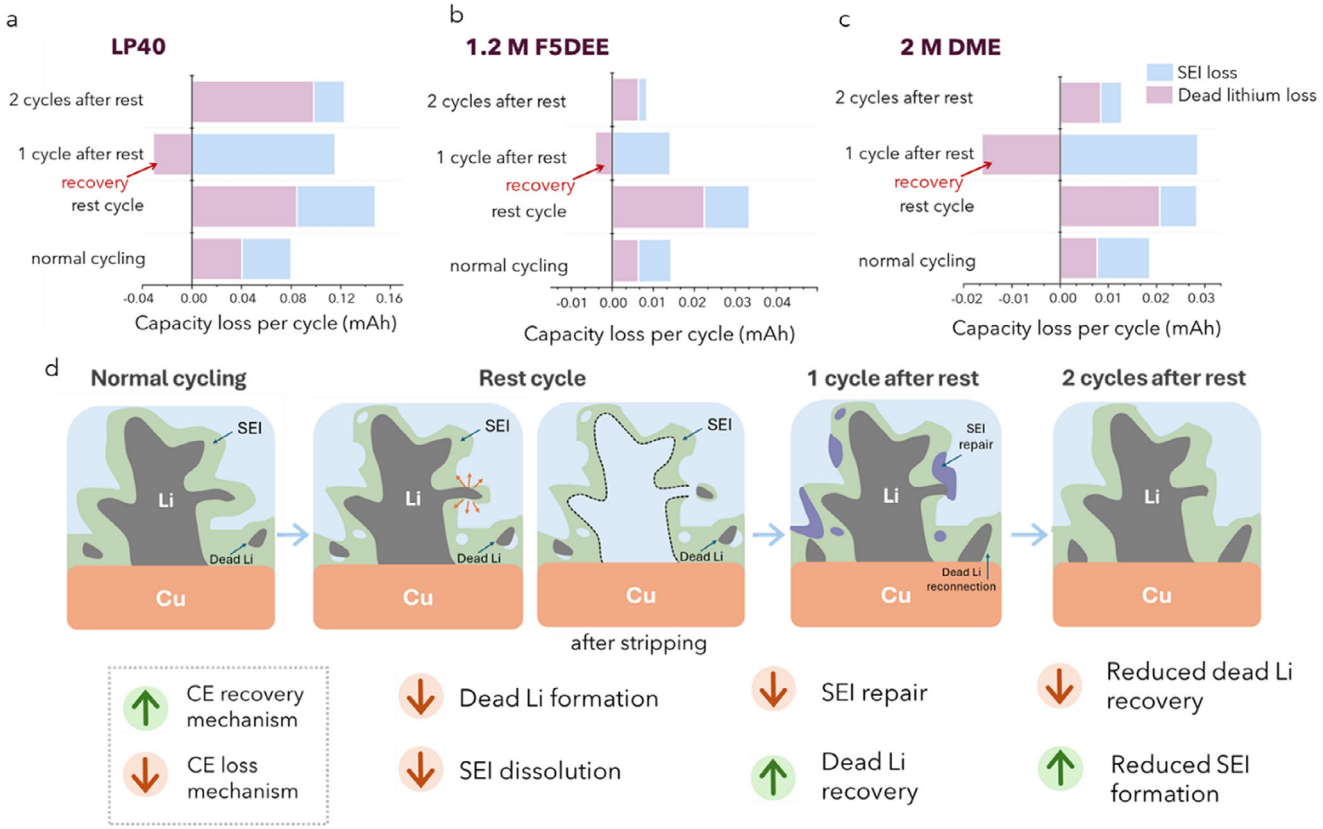

Figure 2. a–c) The capacity loss per cycle divided into SEI and dead lithium contributions for (a) LP40 (b) 1.2 M LiFSI/F5DEE (c) 2 M LiFSI/DME. The capacity loss contributions are tracked for normal cycling, rest cycle, and two consecutive cycles after rest. d) Proposed mechanism illustrating the CE recovery and CE loss mechanisms during and after calendar aging. The green upward arrows represent CE recovery mechanisms, and the orange downward arrows represent the CE loss mechanisms. These mechanisms work together to yield the previously observed CE fluctuation during and after rest.

During normal cycling, the system accumulates both SEI and dead lithium over multiple cycles. When the cell enters the rest cycle at plated state, corrosion of the exposed Li surface starts to take place. Some SEI also begins to dissolve, exposing more lithium surfaces to the electrolyte. These exposed surfaces undergo additional corrosion, creating vulnerable regions in the lithium deposit. These weakened areas often become pinch points during stripping, leading to electrical isolation from the main lithium deposit.[25,29] The combined effect of enhanced dead lithium formation and SEI dissolution results in decreased CE during this cycle. To further probe the role of calendar aging in CE loss, we complemented our TGC measurements with direct imaging of dead lithium deposits using SEM. Figure S12 (Supporting Information) shows representative SEM images of a dead lithium deposit before and after a 24-h rest period. After rest, the deposit surface appears covered by a denser and more uniform layer, suggesting additional SEI formation during the resting step. This observation provides visual evidence that corrosion continues to occur even when the cell is at open circuit, leading to SEI thickening on inactive lithium deposits. Similar behavior has also been captured in previous studies using cryo-TEM, where direct observation of corrosion-induced SEI thickening on aged lithium deposits was reported.[12,30]

The first cycle after rest shows the consequences of prior SEI dissolution and dead Li formation, manifesting in both CE recovery and loss mechanisms. While SEI dissolution enables greater dead lithium recovery (CE recovery),[10] the damaged SEI also requires repair, leading to increased SEI capacity loss as new protective layers form (CE loss). The interplay between these competing effects produces electrolyte-dependent CE trends. In electrolytes prone to significant dead lithium formation, such as LP40, substantial dead lithium recovery during this step produces a net CE increase. However, electrolytes like 1.2 M LiFSI/F5DEE and 2 M LiFSI/DME, which form less dead lithium, may not show immediate CE improvements. This behavior has been shown in Figure 1b, particularly for 1.2 M LiFSI/F5DEE, where no CE jump occurs during initial post-rest cycles. The CE improvement emerges in later cycles as more dead lithium accumulates, enabling greater recovery and corresponding CE gains. We would like to mention that the CE recovery during this cycle may also have alternative possibilities. For instance, Li^0 (metallic lithium) can chemically dissolve into the electrolyte over time. This dissolved lithium may further react with electrolyte, forming SEI components. If dead lithium slowly reacts chemically to form SEI compounds, it's no longer counted as metallic lithium, therefore the total dead lithium amount still appears to be lower.

The second cycle after rest also exhibits competing mechanisms. CE recovery occurs due to reduced SEI capacity loss, a benefit of the extensive SEI formation in the previous cycle. However, CE drop from the previous cycle arises from depleted recoverable dead lithium within the residual SEI. This effect becomes particularly pronounced in LP40, where regular dead lithium recovery occurs during normal cycling. The enhanced recovery during rest depletes the available dead lithium, leaving less for recovery in subsequent cycles. This mechanism explains the cycling trends observed in Figure 1b.

We note that SEI dissolution (a chemical process) and new SEI formation (an electrochemical process) cannot be assumed to be completely decoupled. SEI dissolution occurs primarily during rest through the gradual solubilization of metastable SEI components into the electrolyte. However, freshly exposed lithium surfaces—whether from SEI loss or lithium reconnection—can chemically react with the electrolyte even before current is applied, initiating new SEI growth. For clarity, we describe these as conceptually distinct steps, but in practice they may temporally overlap, particularly at the onset of re-cycling. Importantly, SEI dissolution plays a dual role: it can facilitate reactivation of electronically isolated Li^0 by restoring interfacial contact, yet it can also drive additional SEI growth and potentially leading to new dead lithium formation. The balance between these competing effects depends strongly on the cycling protocol and electrolyte formulation.

1.4. Verifying Proposed Mechanism by Controlling Electrochemical Parameters

This proposed mechanism requires experimental validation. To this end, we systematically vary the two primary factors dominating calendar aging: SEI dissolution and dead lithium formation. By adjusting these parameters, we can verify how each factor influences the calendar aging process. More specifically, we can decrease the SEI dissolution with a higher electrolyte concentration,[11] and increase dead lithium formation with higher current densities (Figure S8, Supporting Information).[31]

We select F5DEE and DME electrolyte systems for these controlled studies. **Figure 3**a,c demonstrates how cycling behavior changes with electrolyte concentration. The CE drop between the 10th and 11th cycles, caused by 24 h of rest, shows clear concentration dependence. At constant current density, lower electrolyte concentrations produced larger CE drops during aging. This observation aligns with our understanding that reduced salt concentration exacerbates SEI dissolution, which in turn accelerates corrosion during rest and increases dead lithium formation during stripping. The effect of salt concentration on SEI dissolution can be understood in terms of solvent–solute interactions. At lower salt concentrations, the electrolyte contains a higher proportion of free (uncoordinated) solvent molecules, which are capable of solvating and dissolving metastable SEI species—particularly organic and lithium-containing components. These interactions can promote SEI thinning during rest.[11] In contrast, in high-concentration electrolytes, the solvent is largely coordinated to Li^+ ions, forming tight solvation shells that significantly reduce the population of free solvent molecules. This reduced solvent activity diminishes the capacity of the electrolyte to solvate and dissolve SEI components, thereby stabilizing the SEI and suppressing its dissolution. To further verify this relationship, we performed additional TGC measurements comparing electrolytes with different salt concentrations. As shown in Figure S14 (Supporting Information), cells with a higher concentration (2 M F5DEE) exhibited less dead lithium growth after a 24-h rest compared to those with 1.2 M F5DEE, confirming that higher concentration helps suppress SEI dissolution and corrosion-driven dead lithium formation.

The enhanced SEI dissolution at lower concentrations also results in more pronounced dead lithium recovery between the 11th and 12th cycles. These trends are quantitatively presented in Figure 3f,h. In both figures, the ΔCE values are calculated to represent the change in CE before and after rest. More specifically, a higher ΔCE 11-10 value (ΔCE between 10th and 11th cycle, this value is negative because of lower CE at the 11th cycle) means less dead Li formation and less SEI dissolution. A higher ΔCE 12-11 value means more dead Li reconnection. Reducing DME concentration from 2 to 1 M decreases the ΔCE 11-10 by ≈0.5% and increases the ΔCE 12-11 by about 0.3%. Similarly, lowering F5DEE concentration from 2 to 1.2 M leads to decrease of roughly 0.4% in ΔCE 11-10 and increase of 0.5% in ΔCE 12-11. These results support our hypothesis that SEI dissolution influences both immediate resting behavior and subsequent cycling performance.

We then examine how current density affects calendar aging dynamics since higher current density will lead to a greater amount of dead lithium formation. Figure 3b,d reveal dramatic changes in CE trends when increasing current density from 0.5 to 1 mA cm^{-2} while maintaining constant electrolyte concentrations (2 M LiFSI/DME and 1.2 M LiFSI/F5DEE). The CE drop from the 10th to the 11th cycle increased significantly at higher current density. This larger drop corresponds to enhanced dead lithium formation during the rest period.

With additional dead lithium formed during the rest cycle, the subsequent cycle's dead lithium recovery also increases substantially. Consequently, we observe a larger CE jump from the 11th to the 12th cycle at higher current density. The quantitative values presented in Figure 3e,g provide direct comparisons of these effects. Both 2 M LiFSI/DME and 1.2 M LiFSI/F5DEE show significant increases in ΔCE 11-10 and ΔCE 12-11 values when current density increased. These findings emphasize the strong influence of dead lithium quantity on calendar aging dynamics.

It is worth noting that our systematic control of SEI dissolution and dead lithium formation through electrolyte concentration and current density, respectively, allows us to verify both aspects of our proposed mechanism. The consistent responses observed across different electrolyte systems strengthen our understanding of how these factors contribute to calendar aging behavior.

The previous discussion of SEI evolution has relied primarily on calculations derived from TGC-determined dead lithium content. While this indirect approach provides valuable insights, direct experimental evidence of rest-induced SEI dissolution and subsequent repair would significantly strengthen the proposed mechanism. To address this need, we developed experimental protocols specifically tailored to study SEI repair behavior. A similar analytical approach, coulometric titration time analysis, has proven successful in solid-state electrolytes to quantify side reactions in lithium metal batteries.[32] In our system, these protocols

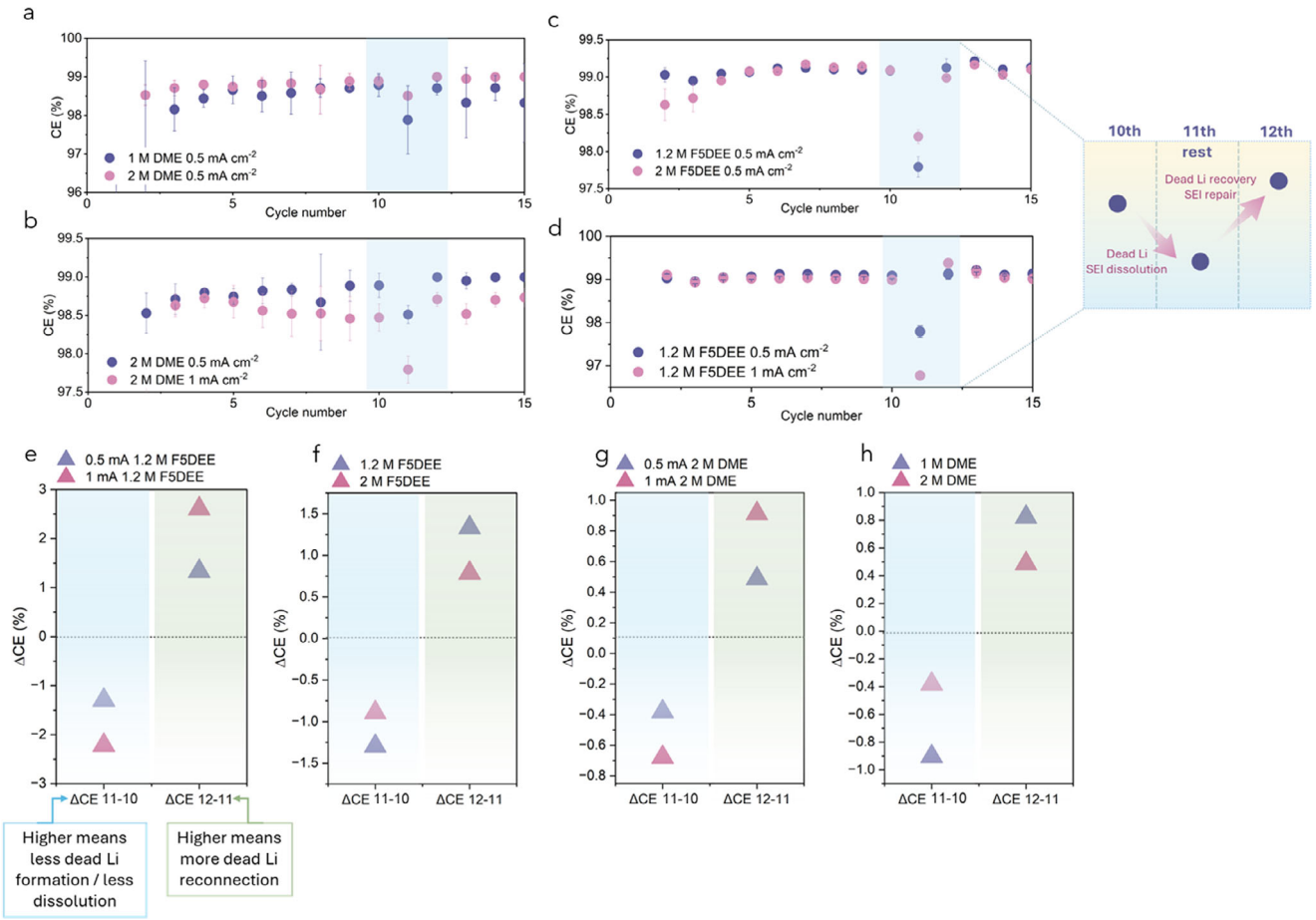

Figure 3. a–d) The Li||Cu cycling profile of DME and F5DEE-based electrolytes, with 24 h of rest applied every ten cycles. The first 15 cycles are shown to reflect how tuning different cycling parameters can influence the CE. The error bars are calculated based on three repeat cells for each condition. a) Li||Cu cells cycled at 0.5 mA cm^{-2} and 1 mAh cm^{-2}. The 2 M LiFSI/DME is compared to 1 M LiFSI/DME. b) Li||Cu cells cycled based on 2 M LiFSI/DME. Cells cycled at 0.5 mA cm^{-2} and 1 mAh cm^{-2} are compared to those cycled at 1 mA cm^{-2} and 1 mAh cm^{-2}. c) Li||Cu cells cycled at 0.5 mA cm^{-2} and 1 mAh cm^{-2}. The 1.2 M LiFSI/F5DEE is compared to 2 M LiFSI/F5DEE. d) Li||Cu cells cycled based on 1.2 M LiFSI/F5DEE. Cells cycled at 0.5 mA cm^{-2} and 1 mAh cm^{-2} are compared to those cycled at 1 mA cm^{-2} and 1 mAh cm^{-2}. e–h) The ΔCE values of the two different electrolytes cycled at 0.5 mA cm^{-2} or 1 mA cm^{-2}. The ΔCE 11-10 is calculated by subtracting the CE of 10th cycle from CE of the 11th cycle. The ΔCE 12-11 value is calculated by subtracting the CE of 11th cycle from CE of the 12th cycle. For the ΔCE 11-10, a higher value means less dead lithium formation and less SEI dissolution. For the ΔCE 12-11, a higher value means more dead lithium reconnection.

provide a direct way to determine whether additional SEI formation becomes necessary when the existing SEI layer experiences damage during rest.

Figure 4a illustrates the experimental design to directly observe SEI repair. Both protocols begin with an identical initial step: forming a stable SEI layer by holding the cell at 10 mV for 12 h. This voltage is selected as it sits above the lithium plating potential while remaining sufficiently low to enable SEI formation.[11] The 12-h duration is essential for establishing a stable, well-formed SEI layer.

In Protocol 1, after SEI formation, a small amount of lithium (10 μAh) is deposited onto the copper substrate. This carefully chosen quantity of lithium serves as a sensitive indicator: when this lithium completely corrodes, the cell system exhibits a characteristic jump in voltage. Protocol 2 introduces a key variation: after the initial SEI formation but before lithium deposition, a 24-h rest period is introduced. This rest period mirrors the conditions used in our long-term cycling studies, allowing a direct comparison with our previous results.

By comparing the timing of the voltage jump between these two protocols, we can evaluate how the rest period affects SEI stability and protection. Figure 4b,c presents comparative results for both 2 M LiFSI/DME and 1.2 M LiFSI/F5DEE electrolyte systems. In both cases, cells that did not experience the 24-h rest period—those with an uncompromised SEI layer—show significantly delayed voltage jumps. This delayed response indicates better protection of the deposited lithium by the intact SEI. Conversely, cells that underwent rest show earlier voltage jumps, demonstrating that SEI dissolution during rest compromises the layer's integrity.

This systematic comparison provides direct evidence that additional SEI formation is required to repair the SEI dissolved during rest. This experimental validation fills an important gap in our understanding, as the SEI repair process after rest periods

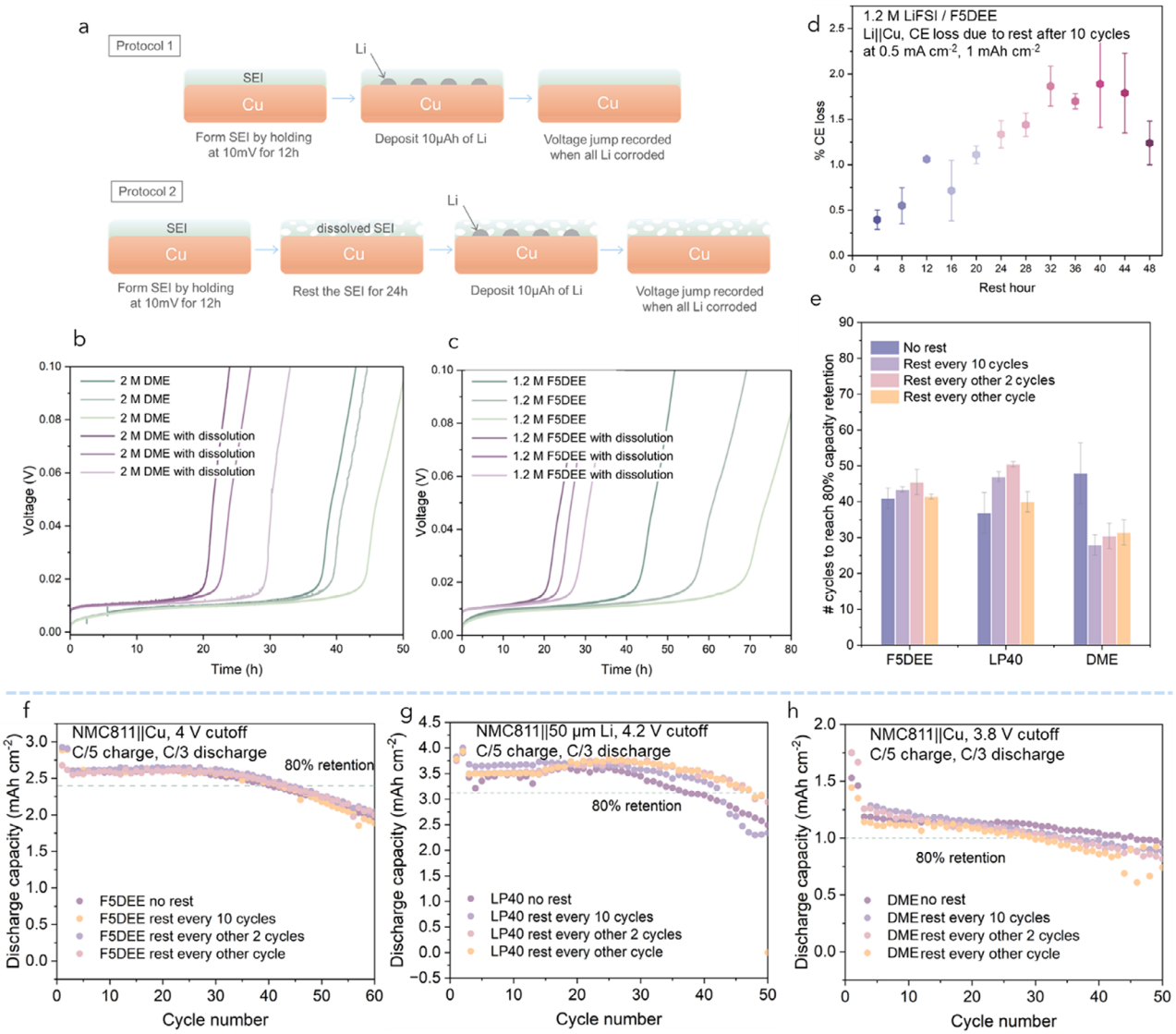

Figure 4. a) Scheme illustrating the two different protocols for determining corrosion of the deposited lithium. The difference between these two protocols is that the SEI is either rested for 24 h or not rested. b,c) The voltage vs time plot of (b) 2 M LiFSI/DME and (c) 1.2 M LiFSI/F5DEE. The longer it takes for voltage to jump up means the longer it takes for the deposited lithium to corrode. Three repeat cells for made for each condition, all of which are shown on the plot. d) The percentage of CE loss after rest vs the resting time. The time varies from 4 to 48 h. The cells are based on 1.2 M LiFSI/F5DEE and are all cycled ten times at 0.5 mA cm^{-2} and 1 mAh cm^{-2} before rest. Three repeat cells are made for each condition and the error bars are shown on the plot. e) The number of cycles for the cells to reach 80% capacity retention for the three different electrolytes rested under different resting frequencies. For 1.2 M F5DEE, Cu||NMC811 cells with 4 V voltage cutoff and 4 mAh cm^{-2} loading are assembled and cycled at C/5 charge and C/3 discharge rate. For 2 M DME, Cu||NMC811 cells with 3.8 V voltage cutoff and 4 mAh cm^{-2} loading are assembled and cycled at C/5 charge and C/3 discharge rate. For LP40, 50 μm Li||NMC811 cells with 4.2 V voltage cutoff and 4 mAh cm^{-2} loading are assembled and cycled at C/5 charge and C/3 discharge rate. Three repeat cells are made for each condition and the error bars are shown on the plot. f–h) The discharge capacity vs cycle number plots for all three electrolytes at different resting frequencies. The 80% retention line is defined by multiplying the average capacity value of the first three cycles by 0.8. This value may differ in different electrolytes because of the different voltage cutoffs.

had not been thoroughly examined in previous studies, despite its essential role in the overall calendar aging mechanism.

1.5. Effect of Cell Resting Time and Implications in Full Cells

Our investigation has yielded two significant findings regarding calendar aging in lithium metal batteries. First, we identified clear electrolyte-dependent patterns in how cells respond to rest periods and subsequent cycling. Second, we uncovered and explained the fundamental mechanisms driving these behaviors, particularly the interplay between dead lithium formation and SEI evolution. These insights, while valuable, emerge from experiments carried out in half cells and using a standardized 24-h rest period. To bridge the gap between these studies and practical applications, it is necessary to examine how these effects are

manifested under various resting durations and in full cell configurations.

We first examine how the length of rest periods affects battery degradation, since real devices experience varying idle times rather than the fixed 24-h period used in our initial studies. To systematically evaluate the impact of resting duration, we examine CE loss across a broad spectrum of rest periods in 1.2 M LiFSI/F5DEE, from 4 to 48 h. Figure 4d reveals a clear correlation between rest duration and capacity loss.

As rest periods extend, CE loss increases progressively, reaching its maximum between 32 and 40 h. Beyond this threshold, further extension of rest time does not induce additional CE loss. This plateau effect carries significant mechanistic implications. The saturation behavior suggests that our identified degradation mechanisms, specifically dead lithium formation and SEI dissolution, reach completion or equilibrium after sufficient time. Rather than continuing indefinitely, these processes appear to have natural limits, consistent with previous findings in the literature.[11]

After examining rest period effects in half cells, we transition our investigation into full cell configurations to understand calendar aging under more practical conditions. This transition to full cells is particularly crucial because, unlike half cells where excess lithium is available, full cells operate with a finite lithium source. While half cells make it difficult to quantify remaining lithium content, full cells enable us to track the cumulative impact of competing processes—both lithium loss through degradation and recovery through reconnection of dead lithium.

To systematically investigate these effects, we implement varying rest frequencies in our cycling protocols. Our experimental design begins with frequent rest periods (every other cycle), then progressively decreases the frequency to every two cycles, and finally to every ten cycles. Based on conventional understanding of corrosion mechanisms,[12] one might expect that more frequent rest periods would accelerate capacity loss, as each rest period provides additional opportunity for corrosion-induced degradation. However, our experimental results reveal a more complex behavior.

Before diving into the results, it is necessary to establish specific cycling protocols for each electrolyte system to isolate rest effects from other degradation mechanisms. For the 1.2 M LiFSI/F5DEE electrolyte, we conduct tests in Cu||NMC811 anode-free cells using 4 mAh cm^{-2} cathodes. We specifically select a 4 V voltage cutoff to eliminate any potential interference from cathode degradation mechanisms. This ensures that our observations purely reflect the impact of calendar aging rather than convolution with cathode instability effects. For 2 M LiFSI/DME, we reduce the voltage cutoff to 3.8 V. This adjustment is necessary to account for DME's lower oxidative stability, preventing any interference from electrolyte decomposition at higher voltages. LP40 presents unique challenges due to its poor reductive stability, necessitating a different cell configuration. Instead of anode-free cells, we employed 50 µm Li||NMC811 cells with 4 mAh cm^{-2} cathodes. This design choice allows for extended cycling periods, enabling clearer observation of cycling trends. The voltage cutoff is set to be at 4.2 V, taking advantage of LP40's superior oxidative stability compared to the ether-based electrolytes. The higher voltage cutoff in this case remains safe due to LP40's established stability at these potentials.[27]

Across all systems, we maintain consistent cycling rates, using C/5 for charging and C/3 for discharging. While each electrolyte system requires its own optimized testing conditions, we ensure absolute consistency of conditions within each electrolyte group. This experimental design isolates resting frequency as the sole variable within each electrolyte system, enabling clear interpretation of rest-induced effects.

Figure 4e demonstrates an unexpected finding: increasing the frequency of rest periods does not correlate with accelerated capacity loss, and the trend also slightly differs in different electrolytes. The detailed discharge capacity curves are shown in Figure 4f,g for each electrolyte (data for repeated cells are shown in Figures S9–S11, Supporting Information). In 1.2 M LiFSI/F5DEE, the number of cycles to reach 80% capacity retention is almost identical across the different resting frequencies. In LP40, we even observed more capacity retention for the most frequently rested cells. It is only in 2 M LiFSI/DME where we see a slight reduction in capacity retention as resting frequency increases. Interestingly, while LP40 forms significantly more dead lithium during rest in Li||Cu cells (Figure 1d), it shows improved capacity retention in full cells under the same conditions (Figure 4e). This apparent discrepancy can be reconciled by considering the reversibility of dead lithium in each system. In LP40, the SEI is generally more organic-rich and chemically soluble, which allows for partial SEI dissolution or reorganization during rest. This can expose previously isolated Li^0, enabling its reconnection and continued electrochemical participation. As a result, much of the dead lithium formed in LP40 may be transient and recoverable, improving overall cycling stability. In contrast, the SEI in DME-based electrolytes is typically more inorganic (e.g., LiF-rich), stable, and less soluble, which may hinder reconnection and make dead lithium formation more irreversible. Consequently, even small amounts of disconnection in DME can lead to permanent lithium loss and capacity degradation. These results suggest that not only the amount but also the reversibility and nature of dead lithium, strongly influenced by SEI composition and solubility, are critical in determining full-cell performance.

The observation that increased resting frequency does not accelerate capacity loss in all electrolyte systems carries significant mechanistic implications. Unlike our previous understanding that calendar aging is detrimental to cycling life, the capacity loss we observe during rest periods can be highly recoverable. Our proposed mechanism offers a potential explanation: while resting periods induce corrosion and lead to dead lithium formation, this dead lithium remains available for recovery in subsequent cycles. The identification of this balance between dead lithium formation and recovery provides crucial insights for electrolyte design and cell engineering. By understanding how different electrolyte systems respond to rest periods, we can better tailor electrolyte compositions and concentrations to maximize recovery capabilities.

2. Conclusion

This study provides comprehensive insights into calendar aging mechanisms in lithium metal batteries, revealing complexities that extend beyond single-cycle rest-induced degradation. We demonstrate that calendar aging effects persist through multiple

cycles after rest, creating a dynamic sequence of degradation and recovery processes that vary significantly with electrolyte chemistry. This finding fundamentally changes our understanding of how lithium metal batteries respond to rest periods.

Through systematic investigation of three representative electrolyte systems—LP40, 1.2 M LiFSI/F5DEE, and 2 M LiFSI/DME—we uncover distinct patterns in how each electrolyte responds to rest periods. Carbonate-based electrolyte LP40 shows significant dead lithium formation during rest but also exhibits notable CE recovery in the subsequent cycle. In contrast, ether-based electrolytes demonstrate different behavior patterns. We found that the CE recovery does not occur right away in 1.2 M LiFSI/F5DEE and 2 M LiFSI/DME. To explain these observations, we identified and verified key mechanisms driving these behaviors. SEI dissolution during rest creates opportunities for dead lithium recovery, while also necessitating additional SEI formation in subsequent cycles. This interplay between SEI evolution and dead lithium dynamics explains the complex patterns observed in post-rest cycling.

We then extend our investigation to full cells, where the finite lithium inventory allows us to track the cumulative effect of calendar aging. Interestingly, increased rest frequency does not necessarily accelerate capacity loss, revealing the recoverable nature of rest-induced degradation. The ability to recover lithium in subsequent cycles plays a crucial role in long-term cell performance.

Beyond experimental observations, simulation studies play a crucial role in elucidating the molecular-level processes that govern electrolyte behavior and interphase evolution. Recent computational work has revealed how variations in solvation structure and ion clustering can strongly influence SEI composition and stability, thereby impacting both CE loss and recovery during rest periods. These insights complement our experimental findings and provide a theoretical framework for understanding the dynamic interplay between electrolyte chemistry and calendar-aging phenomena.[33]

Future work should focus on developing electrolyte systems that can maximize recovery during and after rest periods. This requires careful balancing of SEI dissolution and dead lithium formation; while some SEI dissolution is necessary to enable dead lithium recovery, excessive dissolution can lead to accelerated corrosion. The optimal electrolyte system should maintain sufficient SEI stability while promoting efficient dead lithium recovery mechanisms. Additionally, our findings in full cells provide practical guidelines for optimizing real-world battery systems, particularly in applications involving intermittent use. This improved understanding of calendar aging mechanisms in both half cells and full cells provides a stronger foundation for developing more reliable and efficient lithium metal batteries.

3. Experimental Section

General Materials: LP40 (1 M $LiPF_6$ salt in a 1:1 volume ratio mixture of ethylene carbonate and diethyl carbonate) and DME (1,2-dimethoxyethane) were purchased from Sigma Aldrich or Fisher. F5DEE was synthesized based on the procedure reported previously[21] and provided by Feon Energy. The LiFSI salt was purchased from Solvionic and Arkema. The separator Celgard 2325 (25 µm thick, polypropylene/polyethylene/polypropylene) was purchased from Celgard. Thick Li foil (roughly 600 µm thick) from MSE Supplies and Cu current collector (25 µm thick) were purchased from Alfa Aesar. Commercial NMC811 cathode sheets were purchased from Targray. Additional battery components, including 2032-type coin-cell cases, springs, and spacers, were obtained from MTI. All materials were used as received.

Electrochemical Measurements and Characterizations: All electrochemical measurements were conducted using commercial 2032-type coin cells assembled with readily available battery components. Cell assembly was performed in an argon atmosphere glovebox using Celgard 2325 as the separator material. Unless specified otherwise, lithium foil (750 µm thickness, 7/16 in. diameter) served as the counter electrode, with 40 µL electrolyte added per cell. The Li||Cu, Li||NMC, and Cu||NMC cells were evaluated using a Landt battery testing system at room temperature. For Li||Cu cells, the Cu surface was initially conditioned through ten cycles between 0 and 1 V at 0.2 mA cm^{-2}. Following this preconditioning step, various testing protocols were implemented as detailed in previous sections. Full cells were cycled within voltage ranges of 2.8–3.8 V (2 M DME), 2.8–4 V (1.2 M F5DEE), or 2.8–4.2 V (LP40) using C/5 and C/3 rates for charging and discharging, respectively. All full cells utilized Al-clad cathode cases, with additional Al foil inserted to minimize potential cladding defects.

SEI repair verification was performed using a BioLogic instrument following the two protocols described in the previous sections. Li||Cu half cells underwent initial SEI formation by holding at 10 mV for 12 h. In protocol 1, cells proceeded directly to the next step, while protocol 2 included a 24-h rest period. Subsequently, 10 µAh of lithium was deposited, and the voltage response time was monitored. Dead lithium quantification employed Titration Gas Chromatography. After cycling under previously specified conditions, cells were disassembled to retrieve the Cu electrode. The Cu foil containing residual SEI and dead Li was placed in a 10 mL GC vial within the glovebox and sealed before removal. Analysis involved adding 1 mL of water to the vial, allowing a 3-min reaction period, followed by extraction and GC analysis of 1.5 mL of the evolved gas.

Supporting Information

Supporting Information is available from the Wiley Online Library or from the author.

Acknowledgements

The work was supported by the Assistant Secretary for Energy Efficiency and Renewable Energy, Office of Vehicle Technologies of the U.S. Department of Energy under the Battery 500 Consortium Program. E.Z. acknowledges the support from the National Science Foundation Graduate Research Fellowships Program (NSF GRFP). Part of this work was performed at the Stanford Nano Shared Facilities (SNSF), supported by the National Science Foundation under Award ECCS-2026822. The authors thank Feon Energy for providing F5DEE.

Conflict of Interest

The authors declare no conflict of interest.

Author Contributions

E.Z., Z.B., and Y.C. conceived the idea. E.Z. conducted the experiments and analyzed all results under the guidance of Z.B. and Y.C. H.L., Y.C., W.Z., P.S., and I.R.C. contributed to discussions and assisted in developing experimental procedures. E.Z. wrote the manuscript. Z.B. and Y.C. directed this work. All authors discussed the results and commented on the manuscript.

Data Availability Statement

The data that support the findings of this study are available in the supplementary material of this article.

Keywords

battery, calendar aging, electrolytes, lithium metal batteries

Received: July 19, 2025
Revised: September 30, 2025
Published online:

[1] J. Liu, Z. Bao, Y. Cui, E. J. Dufek, J. B. Goodenough, P. Khalifah, Q. Li, B. Y. Liaw, P. Liu, A. Manthiram, Y. S. Meng, V. R. Subramanian, M. F. Toney, V. V. Viswanathan, M. S. Whittingham, J. Xiao, W. Xu, J. Yang, X.-Q. Yang, J.-G. Zhang, *Nat. Energy* **2019**, *4*, 180.
[2] D. Lin, Y. Liu, Y. Cui, *Nat. Nanotechnol.* **2017**, *12*, 194.
[3] X. Shen, H. Liu, X.-B. Cheng, C. Yan, J.-Q. Huang, *Energy Storage Mater.* **2018**, *12*, 161.
[4] P. Albertus, S. Babinec, S. Litzelman, A. Newman, *Nat. Energy* **2017**, *3*, 16.
[5] F. M. N. U. Khan, M. G. Rasul, A. S. M. Sayem, N. K. Mandal, *J. Energy Storage* **2023**, *71*, 108033.
[6] M. He, L. G. Hector, F. Dai, F. Xu, S. Kolluri, N. Hardin, M. Cai, *Nat. Energy* **2024**, *9*, 1199.
[7] Y. Zhu, V. Pande, L. Li, B. Wen, M. S. Pan, D. Wang, Z.-F. Ma, V. Viswanathan, Y.-M. Chiang, *Proc. Natl. Acad. Sci. USA* **2020**, *117*, 27195.
[8] L. Yang, N. M. Hagh, J. Roy, E. Macciomei, J. R. Klein, U. Janakiraman, M. E. Fortier, *J. Electrochem. Soc.* **2024**, *171*, 060504.
[9] X.-B. Cheng, R. Zhang, C.-Z. Zhao, Q. Zhang, *Chem. Rev.* **2017**, *117*, 10403.
[10] W. Zhang, P. Sayavong, X. Xiao, S. T. Oyakhire, S. B. Shuchi, R. A. Vilá, D. T. Boyle, S. C. Kim, M. S. Kim, S. E. Holmes, Y. Ye, D. Li, S. F. Bent, Y. Cui, *Nature* **2024**, *626*, 306.
[11] P. Sayavong, W. Zhang, S. T. Oyakhire, D. T. Boyle, Y. Chen, S. C. Kim, R. A. Vilá, S. E. Holmes, M. S. Kim, S. F. Bent, Z. Bao, Y. Cui, *J. Am. Chem. Soc.* **2023**, *145*, 12342.
[12] D. T. Boyle, W. Huang, H. Wang, Y. Li, H. Chen, Z. Yu, W. Zhang, Z. Bao, Y. Cui, *Nat. Energy* **2021**, *6*, 487.
[13] L. C. Merrill, S. G. Rosenberg, K. L. Jungjohann, K. L. Harrison, *ACS Appl. Energy Mater.* **2021**, *4*, 7589.
[14] L. C. Merrill, D. M. Long, S. G. Rosenberg, M. L. Meyerson, M. N. Lam, K. L. Harrison, *Front. Batter. Electrochem.* **2023**, *2*, 1293877.
[15] S. M. Wood, C. Fang, E. J. Dufek, S. C. Nagpure, S. V. Sazhin, B. Liaw, Y. S. Meng, *Adv. Energy Mater.* **2018**, *8*, 1801427.
[16] X. Cao, Y. Xu, L. Zou, J. Bao, Y. Chen, B. E. Matthews, J. Hu, X. He, M. H. Engelhard, C. Niu, B. W. Arey, C. Wang, J. Xiao, J. Liu, C. Wang, W. Xu, J.-G. Zhang, *Energy Environ. Sci.* **2023**, *16*, 1548.
[17] J. Seara, F. Alcaide, V. L. Barrio, A. Benayad, E. Ayerbe, *J. Electrochem. Soc.* **2022**, *169*, 080526.
[18] K. L. Bassett, K. A. Small, D. M. Long, L. C. Merrill, B. Warren, K. L. Harrison, *Front. Batter. Electrochem.* **2023**, *2*, 1292639.
[19] S. Kim, P. Barnes, H. Zhang, C. Efaw, Y. Wang, B. Park, B. Li, B.-R. Chen, M. C. Evans, B. Liaw, D. Olds, P. G. Khalifah, E. J. Dufek, *Energy Storage Mater.* **2024**, *65*, 103147.
[20] A. B. Gunnarsdóttir, C. V. Amanchukwu, S. Menkin, C. P. Grey, *J. Am. Chem. Soc.* **2020**, *142*, 20814.
[21] Z. Yu, P. E. Rudnicki, Z. Zhang, Z. Huang, H. Celik, S. T. Oyakhire, Y. Chen, X. Kong, S. C. Kim, X. Xiao, H. Wang, Y. Zheng, G. A. Kamat, M. S. Kim, S. F. Bent, J. Qin, Y. Cui, Z. Bao, *Nat. Energy* **2022**, *7*, 94.
[22] H. Wang, Z. Yu, X. Kong, S. C. Kim, D. T. Boyle, J. Qin, Z. Bao, Y. Cui, *Joule* **2022**, *6*, 588.
[23] J. Xiao, Q. Li, Y. Bi, M. Cai, B. Dunn, T. Glossmann, J. Liu, T. Osaka, R. Sugiura, B. Wu, J. Yang, J.-G. Zhang, M. S. Whittingham, *Nat. Energy* **2020**, *5*, 561.
[24] B. Lu, W. Li, D. Cheng, B. Bhamwala, M. Ceja, W. Bao, C. Fang, Y. S. Meng, *Adv. Energy Mater.* **2022**, *12*, 2202012.
[25] C. Fang, J. Li, M. Zhang, Y. Zhang, F. Yang, J. Z. Lee, M.-H. Lee, J. Alvarado, M. A. Schroeder, Y. Yang, B. Lu, N. Williams, M. Ceja, L. Yang, M. Cai, J. Gu, K. Xu, X. Wang, Y. S. Meng, *Nature* **2019**, *572*, 511.
[26] R. A. Vilá, D. T. Boyle, A. Dai, W. Zhang, P. Sayavong, Y. Ye, Y. Yang, J. A. Dionne, Y. Cui, *Sci. Adv.* **2023**, *9*, adf3609.
[27] J. Liu, S. Ihuaenyi, R. Kuphal, J. Salinas, L. Xie, L. Yang, U. Janakiraman, M. E. Fortier, C. Fang, *J. Electrochem. Soc.* **2023**, *170*, 010535.
[28] E. Zhang, Y. Chen, J. Holoubek, Z. Yu, W. Zhang, H. Lyu, I. R. Choi, S. C. Kim, C. Serrao, Y. Cui, Z. Bao, *Proc. Natl. Acad. Sci. USA* **2025**, *122*, 2418623122.
[29] Y. Li, W. Huang, Y. Li, A. Pei, D. T. Boyle, Y. Cui, *Joule* **2018**, *2*, 2167.
[30] O. Sheng, J. Zheng, Z. Ju, C. Jin, Y. Wang, M. Chen, J. Nai, T. Liu, W. Zhang, Y. Liu, X. Tao, *Adv. Mater.* **2020**, *32*, 2000223.
[31] Y. Wang, D. Dang, X. Xiao, Y.-T. Cheng, *Energy Storage Mater.* **2020**, *26*, 276.
[32] B. Aktekin, L. M. Riegger, S.-K. Otto, T. Fuchs, A. Henss, J. Janek, *Nat. Commun.* **2023**, *14*, 6946.
[33] T. Yang, Y. Zheng, Y. Liu, D. Luo, A. Yu, Z. Chen, *Renewables* **2023**, *1*, 2.